ISOGEOMETRIC ANALYSIS OF FGM PLATES

Samir P. Auad [(1)], Jamires S. C. Praciano[(1)], Elias S. Barroso[(1)], João B. M. Sousa Jr. [(1)] and Evandro Parente Jr. [(1)]

(1) Departamento de Engenharia Estrutural e Construção Civil, Universidade Federal do Ceará, Brazil

https://doi.org/10.21452/bccm4.2018.16.09

Abstract

This work presents an isogeometric formulation for the geometrically nonlinear analysis of functionally graded material (FGM) plates. FGM plates are made of a mixture of two components (ceramic and metal) whose volume fractions vary smoothly along the thickness. The kinematic model is based on the Reissner-Mindlin theory for bending and shear strains and the von Kármán theory for nonlinear membrane strains. Non-Uniform Rational B-splines (NURBS) are used as basis functions for the isogeometric formulation. The formulation is applied to study the buckling and post-buckling of FGM plates.

1. INTRODUCTION

In light of technological development, especially within the spectrum of engineering applications, the search for new materials, which can perform well under the most diverse and rigorous conditions, plays an important role.

Functionally Graded Materials (FGM) are advanced materials of the composite family. These materials consist of two or more different components, forming a continuous and smooth varying spatial profile. In the preferred orientation, FGM properties (such as Young's modulus and Poisson's ratio) have superior performance in comparison with the isolated constituents and possess mechanical and thermal advantages, such as toughness and a high degree of temperature resistance [1,2].

Due to its thermo-mechanical properties, FGM have a vast application in the manufacture of structural components, in particular, plate elements. Thus, the mechanical behavior of FGM plates has received considerable attention [3-12]. In these studies, nonlinearity and shear effects are some important factors and need to be taken into account.

The Isogeometric Analysis (IGA) is a numerical method proposed by Hughes et al. [13] in order to integrate the numerical analysis and Computer Aided Design (CAD). In IGA, the same basis functions (e.g. NURBS) functions are used for geometric modeling and approximation of the

displacement field. Therefore, the geometry is exactly represented in the structural analysis, independent of the discretization level. In addition, the analysis model can be easily refined using standard geometric modeling algorithms, as knot-insertion and degree-elevation [14].

This work presents an accurate and efficient isogeometric formulation for geometrically nonlinear analysis of FGM plates and shallow shells based on the Reissner-Mindlin plate theory and von Kármán strains. This formulation will be applied in the stability analysis of perfect FGM plates, including the evaluation of the buckling load and post-buckling paths.

2. FUNCTIONALLY GRADED MATERIALS

FGM are obtained by mixing two distinct material phases, as a ceramic and a metal. The manufacture techniques allow a smooth variation of the volume fraction along the thickness direction. Thus, FGM do not present the high stress discontinuities present in conventional laminates.

The ceramic volume fraction (V_c) is assumed to vary in the thickness direction (z) according to a simple power law:

$$V_c(z) = \left(\frac{1}{2} + \frac{z}{h}\right)^n \tag{1}$$

where n is the volume fraction index and h is the plate thickness. The effective material properties can be evaluated by the rule of mixtures [15]:

$$\begin{aligned} E(z) &= E_m + (E_c + E_m)V_c(z) \\ \nu(z) &= \nu_m + (\nu_c + \nu_m)V_c(z) \end{aligned} \tag{2}$$

where E represent Young's modulus, ν represents the Poisson's ratio, and the subscripts m and c represent metal and ceramic, respectively.

3. ISOGEOMETRIC ANALYSIS

The model adopted in this work is based on the Reissner-Mindlin theory for bending and transverse shear strains and the von Kármán theory for nonlinear membrane strains. Thus, the displacement field at any point of the shell is given by:

$$u_x(x,y,z) = u(x,y) + z\theta_y;\;\; u_y(x,y,z) = v(x,y) - z\theta_x; \qquad u_z(x,y,z) = w(x,y) \tag{3}$$

where u, v and w are the midsurface displacements in the x, y, and z directions, respectively.

Using the von Kármán theory, the in-plane strains are given by:

$$\boldsymbol{\varepsilon} = \begin{Bmatrix} \frac{\partial u}{\partial x} \\ \frac{\partial v}{\partial x} \\ \frac{\partial u}{\partial y} + \frac{\partial v}{\partial x} \end{Bmatrix} + \begin{Bmatrix} \frac{1}{2}\left(\frac{\partial w}{\partial x}\right)^2 \\ \frac{1}{2}\left(\frac{\partial w}{\partial y}\right)^2 \\ \left(\frac{\partial w}{\partial x}\right)\left(\frac{\partial w}{\partial y}\right) \end{Bmatrix} + z \begin{Bmatrix} \frac{\partial \theta_y}{\partial x} \\ -\frac{\partial \theta_x}{\partial x} \\ \frac{\partial \theta_y}{\partial x} - \frac{\partial \theta_x}{\partial x} \end{Bmatrix} = \boldsymbol{\varepsilon}^m + z\boldsymbol{\kappa} \tag{4}$$

where $\boldsymbol{\varepsilon}^m$ are the membrane strains and $\boldsymbol{\kappa}$ are the curvatures. According to the Reissner-Mindlin theory, the transverse shear strains are given by:

$$\boldsymbol{\gamma} = \begin{Bmatrix} \gamma_{xz} \\ \gamma_{yz} \end{Bmatrix} = \begin{Bmatrix} \frac{\partial w}{\partial x} + \theta_y \\ \frac{\partial w}{\partial y} - \theta_x \end{Bmatrix} \tag{5}$$

where θ_x and θ_y represents the rotations about the *y* and *x* axes, respectively.

Considering a linear elastic behavior:

$$\begin{Bmatrix} \sigma_x \\ \sigma_y \\ \tau_{xy} \\ \tau_{xz} \\ \tau_{yz} \end{Bmatrix} = \begin{bmatrix} Q_{11} & Q_{12} & 0 & 0 & 0 \\ Q_{12} & Q_{22} & 0 & 0 & 0 \\ 0 & 0 & Q_{66} & 0 & 0 \\ 0 & 0 & 0 & Q_{44} & 0 \\ 0 & 0 & 0 & 0 & Q_{55} \end{bmatrix} \begin{Bmatrix} \varepsilon_x \\ \varepsilon_y \\ \gamma_{xy} \\ \gamma_{xz} \\ \gamma_{yz} \end{Bmatrix} \tag{6}$$

where:

$$Q_{11} = \frac{E}{1-v^2} \qquad Q_{12} = vQ_{11} \quad Q_{22} = Q_{11} \qquad Q_{44} = Q_{55} = Q_{66} = \frac{E}{2(1-v)} \tag{7}$$

The membrane (**N**), bending (**M**) and shear ($\mathbf{Q}_s$) stress resultants are given by:

$$\mathbf{N} = \begin{Bmatrix} N_x \\ N_y \\ N_x \end{Bmatrix} = \int_{-h/2}^{h/2} \begin{Bmatrix} \sigma_{xx} \\ \sigma_{yy} \\ \sigma_{xy} \end{Bmatrix} dz \qquad \mathbf{M} = \begin{Bmatrix} M_x \\ M_y \\ M_{xy} \end{Bmatrix} = \int_{-h/2}^{h/2} \begin{Bmatrix} \sigma_{xx} \\ \sigma_{yy} \\ \sigma_{xy} \end{Bmatrix} z\, dz$$
$$\mathbf{Q}_s = \begin{Bmatrix} Q_{xz} \\ Q_{yz} \end{Bmatrix} = \int_{-h/2}^{h/2} \begin{Bmatrix} \tau_{xz} \\ \tau_{yz} \end{Bmatrix} dz \tag{8}$$

The stress resultants can be written in terms of the generalized strains as:

$$\begin{Bmatrix} \mathbf{N} \\ \mathbf{M} \\ \mathbf{Q} \end{Bmatrix} = \begin{bmatrix} \mathbf{A} & \mathbf{B} & \mathbf{0} \\ \mathbf{B} & \mathbf{D} & \mathbf{0} \\ \mathbf{0} & \mathbf{0} & \mathbf{G} \end{bmatrix} \begin{Bmatrix} \boldsymbol{\varepsilon}^m \\ \boldsymbol{\kappa} \\ \boldsymbol{\gamma} \end{Bmatrix} \tag{9}$$

where **A**, **B**, **D** and **G** are the extensional, membrane-bending coupling, bending and shear stiffness matrices, respectively, given by:

$$\left(A_{ij}, B_{ij}, D_{ij}\right) = \int_{-h/2}^{h/2} Q_{ij}(1, z, z^2) dz \qquad G_{ij} = k_s \int_{-h/2}^{h/2} Q_{ij} dz \tag{10}$$

where k_s denotes the transverse shear correction coefficient and the value 5/6 is adopted. It is important to note that **A**, **B** and **D** are defined for *i*,*j* = 1,2,6 and **G** is defined for *i*,*j* = 4,5.

3.2 NURBS

Non-Uniform Rational B-splines (NURBS) are widely used by CAD systems to model complex geometries. This item provides only the basics required for the present paper and the interest in the reader is referred to [14].

The B-spline basis functions are defined by the recursive Cox-de Boor formula:

$$N_{i,0}(\xi) = \begin{cases} 1, & \xi_i \leq \xi \geq \xi_{i+1} \\ 0, & otherwise \end{cases}$$
$$N_{i,0}(\xi) = \frac{\xi - \xi_i}{\xi_{i+p} - \xi_i} N_{i,p-1}(\xi) + \frac{\xi_{i+p+1} - \xi}{\xi_{i+p+1} - \xi_{i+1}} N_{i+1,p-1}(\xi) \tag{11}$$

However, B-Splines may be insufficient to exactly model curved geometries, as circles and cylinders. In this case, they can be exactly represented by non-uniform rational B-splines (NURBS) functions. The NURBS functions can be defined as:

$$R = \frac{w_{ij} N_{i,p}(\xi) N_{j,q}(\eta)}{W} \qquad W = \sum_{\hat{j}=1}^{m} \sum_{\hat{i}=1}^{n} w_{\hat{i}\hat{j}} N_{\hat{i},p}(\xi) N_{\hat{j},q}(\eta) \tag{12}$$

where ξ and h are two parametric dimensions and p and q are the B-splines basis of degrees in these dimensions, respectively.

A tensor product NURBS surface of degree (p x q) is defined by a linear combination of bivariate rational blending functions (R) and a matrix of control points **p**:

$$\mathbf{S}(\xi, \eta) = \sum_{i=1}^{m} \sum_{j=1}^{n} R_{ij} \mathbf{p}_{ij} \tag{13}$$

In this work, the plate geometry described by a bivariate NURBS surface given by:

$$x = \sum_{k=1}^{nn} R_k x_k \qquad y = \sum_{k=1}^{nn} R_k y_k \tag{14}$$

In the isogeometric formulation presented here, the same NURBS basis are also employed to approximate the membrane and transverse displacements and rotations of the shell:

$$\mathbf{u} = \mathbf{R}\mathbf{u}_e \qquad \mathbf{R} = [\mathbf{R}_1 \ \mathbf{R}_2 \ \cdots \ \mathbf{R}_{\mathrm{nn}}] \qquad \mathbf{R}_k = \mathrm{R}_k \mathbf{I}_{5\mathrm{x}5} \tag{15}$$

where $\mathbf{u} = [u \ v \ w \ \theta_x \ \theta_y]$ is the displacement vector of the midsurface, $\mathbf{u}_e$ is the control points displacements, **R** is the matrix of shape functions and *nn* is the number of control points. Using Equations (4) and (15), the strains can be written as:

$$\boldsymbol{\varepsilon} = \begin{Bmatrix} \boldsymbol{\varepsilon}^m \\ \boldsymbol{\kappa} \\ \boldsymbol{\gamma} \end{Bmatrix} = \begin{Bmatrix} \boldsymbol{\varepsilon}_0^m \\ \boldsymbol{\kappa} \\ \boldsymbol{\gamma} \end{Bmatrix} + \frac{1}{2} \begin{Bmatrix} \boldsymbol{\varepsilon}_L^m \\ \mathbf{0} \\ \mathbf{0} \end{Bmatrix} = \left(\mathbf{B}_0 + \frac{1}{2} \mathbf{B}_L \right) \mathbf{u}_e = \mathbf{B}\mathbf{u}_e \tag{16}$$

where the sub-matrices of **B** for each control point are given by:

$$\mathbf{B}_0^m = \begin{bmatrix} R_{k,x} & 0 & 0 & 0 & 0 \\ 0 & R_{k,x} & 0 & 0 & 0 \\ R_{k,x} & R_{k,x} & 0 & 0 & 0 \end{bmatrix} \qquad \mathbf{B}_0^b = \begin{bmatrix} 0 & 0 & 0 & 0 & R_{k,x} \\ 0 & 0 & 0 & -R_{k,y} & 0 \\ 0 & 0 & 0 & -R_{k,x} & R_{k,y} \end{bmatrix}$$

$$\mathbf{B}_L^m = \begin{bmatrix} 0 & 0 & W_x R_{k,x} & 0 & 0 \\ 0 & 0 & W_y R_{k,x} & 0 & 0 \\ 0 & 0 & W_y R_{k,x} + W_x R_{k,x} & 0 & 0 \end{bmatrix} \qquad \mathbf{B}_0^s = \begin{bmatrix} 0 & 0 & R_{k,x} & 0 & R_k \\ 0 & 0 & R_{k,y} & R_k & 0 \end{bmatrix} \tag{17}$$

with

$$W_x = \sum_{k=1}^{nn} R_{k,x} w_k \qquad W_y = \sum_{k=1}^{nn} R_{k,y} w_k \tag{18}$$

The internal forces vector **g** is derived from the Principle of Virtual Work using the Total Lagragian approach:

$$\mathbf{g}(\mathbf{u}) = \int_{A_0} \overline{\mathbf{B}}^T \hat{\boldsymbol{\sigma}} dA_0 \, , \overline{\mathbf{B}} = (\mathbf{B}_0 + \mathbf{B}_L) \tag{19}$$

The tangent stiffness matrix ($\mathbf{K}_T$) is given by:

$$\mathbf{K}_T = \frac{\partial \mathbf{g}(\mathbf{u})}{\partial \mathbf{u}} = \int_{A_0} \overline{\mathbf{B}}^T \frac{\partial \widehat{\boldsymbol{\sigma}}}{\partial \mathbf{u}} dA_0 + \int_{A_0} \frac{\partial \overline{\mathbf{B}}^T}{\partial \mathbf{u}} \widehat{\boldsymbol{\sigma}} dA_0 \tag{20}$$

where the first term is the material stiffness matrix $\mathbf{K}_L$ and the second term corresponds to the geometric stiffness matrix $\mathbf{K}_\sigma$, given by:

$$\begin{aligned} \mathbf{K}_L &= \int_{A_0} \overline{\mathbf{B}}^T \frac{\partial \widehat{\boldsymbol{\sigma}}}{\partial \mathbf{x}} dA_0 = \int_{A_0} \overline{\mathbf{B}}^T \frac{\partial \widehat{\boldsymbol{\sigma}}}{\partial \boldsymbol{\varepsilon}} \frac{\partial \boldsymbol{\varepsilon}}{\partial \mathbf{u}} dA_0 = \int_{A_0} \overline{\mathbf{B}}^T \mathbf{C}_T \overline{\mathbf{B}} dA_0 \\ \mathbf{K}_\sigma &= \int_{A_0} \frac{\partial \overline{\mathbf{B}}^T}{\partial \mathbf{u}} \widehat{\boldsymbol{\sigma}} dA_0 = \int_{A_0} \frac{\partial \overline{\mathbf{B}}^T}{\partial \mathbf{u}} \mathbf{N} dA_0 = \int_{A_0} \mathbf{G}^T \mathbf{S} \mathbf{G} dA_0 \end{aligned} \tag{21}$$

where:

$$\mathbf{G} = \begin{bmatrix} 0 & 0 & R_{k,x} & 0 & 0 \\ 0 & 0 & R_{k,y} & 0 & 0 \end{bmatrix} \qquad \mathbf{S} = \begin{bmatrix} N_x & N_{xy} \\ N_{xy} & N_y \end{bmatrix} \tag{22}$$

The equilibrium equations for displacement independent loads can be written as:

$$\mathbf{r}(\mathbf{u}, \lambda) = \mathbf{g}(\mathbf{u}) - \lambda \mathbf{f} = \mathbf{0} \tag{23}$$

where **f** is the reference vector for external loads, λ is load factor, and **r** is the residual vector. The nonlinear equilibrium paths (i.e. load-displacement curves) can be traced using appropriate path-following methods, as the Displacement Control or Arc-Length Method [15].

For stability analysis, critical points (limit or bifurcation) along the equilibrium path can be determined solving the nonlinear system:

$$\begin{bmatrix} \mathbf{r}(\mathbf{u}, \lambda) \\ \mathbf{K}(\mathbf{u}, \lambda)\boldsymbol{\varphi} \\ \|\boldsymbol{\varphi}\| - \mathbf{1} \end{bmatrix} = \mathbf{0} \tag{24}$$

The numerical algorithms presented in [16] can be used to the stability analysis of perfect and imperfect structures, including the branch-switching to secondary paths at bifurcation points.

4. NUMERICAL RESULTS

Simply supported (SS) and a clamped (C) FGM plates under uniaxial compressive loading were analyzed using the proposed IGA formulation. The plates are square with length a = 2m and thickness h = 0.02m (h/a = 1/100). The materials properties are: E_m = 70 GPa (metal) and E_c = 380 GPa (ceramic). Poisson's ratio is considered constant and chosen as $\nu = 0.3$. The volume fraction variation along the thickness is illustrated in Figure 1a.

The load is applied at *x*-direction (Figure 1a). In the simply supported (SS) case are all edges fixed in *z*-direction. The nodes at the middle point of loaded and transverse edges are fixed in *y* and *x* directions, respectively. In addition, when all edges are clamped, the rotations about *y* and *x* axes are fixed along the loaded and transverse edges, respectively. These boundary conditions are illustrated in Figure 1a. The IGA model used in the analysis of the FGM plates has 8x8 elements with cubic basis functions (p = 3).

The results are compared with Finite Elements Method (FEM) solution obtained using Abaqus software [17]. Since Abaqus does not have FGM in the materials options, the stiffness matrices **A**, **B**, **D**, and **G** were evaluated in an external routine and given as input data. The analysis was carried out using a 16x16 mesh of quadratic S8R elements.

Several studies about the influence of boundary conditions in FGM plates have been presented in the literature. These works showed the inexistence of bifurcation buckling in simply supported (SS) plates subjected to in-plane compressive edge loads [18], as also occurs for non-symmetric

laminated plates. Therefore, only the clamped (C) case was considered in the bifurcation analysis (linearized buckling), since plates with all edges clamped exhibit bifurcation buckling [19].

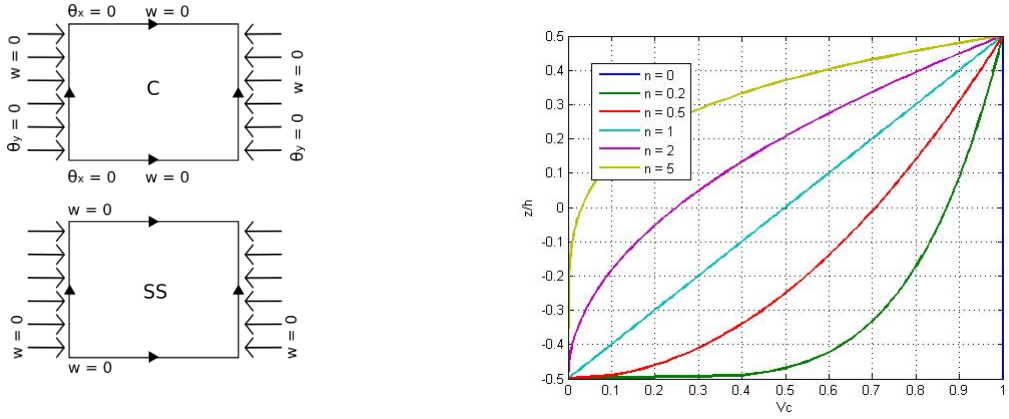

(a) (b)

Figure 1: Boundary conditions and volume fraction along the thickness.

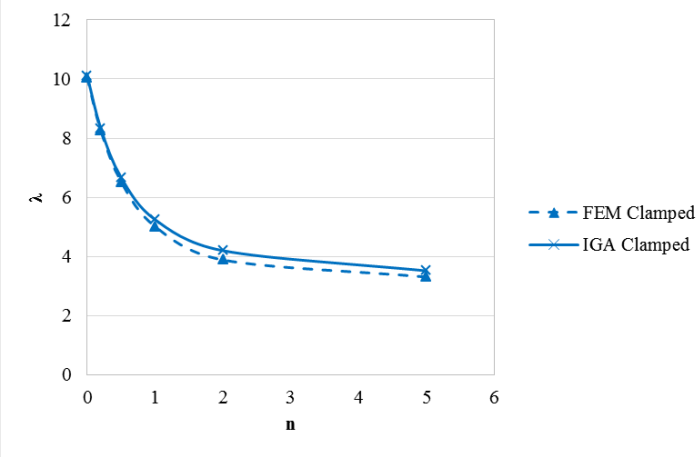

Figure 2: Buckling loads for different exponents.

The obtained results are given in Figure 2, where the normalized buckling coefficient is defined as $\lambda = N_{cr}a^2/\pi^2 D_0$, where $D_0 = Eh^3/12(1-v^2)$. Good agreement is obtained between the IGA and FEM results. The results clearly show that the buckling load decreases with the volume fraction exponent (n).

4.2 Nonlinear analysis

The proposed IGA formulation is used for geometrically nonlinear analysis of FGM plates. The obtained results for simply supported plates are presented in Figure 3a. The load factor is normalized as $\lambda = N_{cr}/N_c$, where N_c is the buckling load of the plate with homogeneous ceramic section (n = 0).

The results show that bifurcation buckling occurs only for $n = 0$ (isotropic plate), since $n > 0$ results in a non-symmetric stiffness distribution leading to stable equilibrium paths, similar to the behavior of imperfect plates. In addition, the results show that increasing the volume fraction exponent (n) decreases the plate strength.

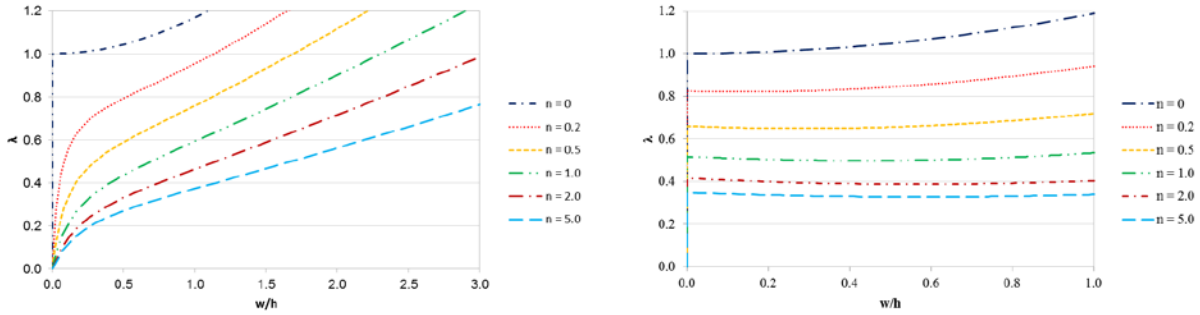

(a) Simply Supported. (b) Clamped.

Figure 3: Nonlinear paths.

The results obtained for clamped plates are presented in Figure 3b. The results show that clamped FGM plates present bifurcation buckling, unlike simple supported ones. In addition, increasing the volume fraction exponent (n) not only decreases the buckling load, but also decreases the post-critical strength reserve of FGM plates, leading to post-buckling behavior characterized by small imperfection sensitivity. This imperfection sensitivity increases with the volume fraction exponent (n).

5. CONCLUSIONS

In this paper, the buckling and post-buckling behavior of FGM plates under uniaxial loading were studied using a NURBS-based isogeometric formulation. Plate kinematics is based on Reissner-Middlin plate theory with the geometrically nonlinear effects considered using the von Kármán theory.

FGM plates with simply supported and clamped boundary conditions were analyzed. The linearized buckling loads for clamped FGM plates computed by the IGA formulation are in good agreement with FEM results. The buckling loads decrease with the volume fraction exponent.

The nonlinear equilibrium paths confirmed that FGM plates with simply supported boundary conditions do not present bifurcation buckling and display a stable nonlinear behavior similar to imperfect homogeneous and laminated plates. On the other hand, clamped FGM plates present bifurcation buckling, but display a slight imperfection sensitivity, which increases with the volume fraction exponent.

ACKNOWLEDGEMENTS

The financial support by CNPq and CAPES is gratefully acknowledged.

REFERENCES

[1] Jha, D. K., Kant, T., & Singh, R. K. (2013), 'A critical review of recent research on functionally graded plates', *Composite Structures*, **96**, (2013) 833-849.

[2] Udupa, G., Rao, S. S., & Gangadharan, K. V., 'Functionally Graded Composite Materials: An Overview', *Procedia Materials*, **5**, (2014) 1291-1299.
[3] Arciniega, R. A., & Reddy, J. N., 'Large deformation anlysis of functionally graded shells', International Journal of Solids and Structures, **44** (6), (2007) 2036-2052.
[4] Lee, Y. Y., Zhao, X., & Reddy, J. N., 'Postbuckling analysis of functionally graded plates subject to compressive and thermal loads', *Computer Methods in Applied Mechanics and Engineering*, **199** (25-28), (2010) 1645-1653.
[5] Woo, J., Meguid, S.A., Stranart, J. C., & Liew, K. M., 'Thermomechanical postbuckling analysis of moderately thick functionally graded plates and shallow shells', *International Journal of Mechanical Sciences*, **47** (8), (2005) 1147-1171.
[6] Yang, J., & Shen, H.-S., 'Non-linear analysis of functionally graded plates under transverse and in-plane loads. *International Journal of Non-Linear Mechanics*', **38** (4), (2003a) 467-482.
[7] Yang, J., & Shen, H. S., 'Nonlinear bending analysis of shear deformable functionally graded plates subjected to thermo-mechanical loads under various boundary conditions', *Composites Part B: Engineering*, **24** (2), (2003b) 103-115.
[8] Zhao, X., Lee, Y. Y., & Liew, K. M., 'Mechanical and thermal buckling analysis of functionally graded plates', *Composite Structures*, **90** (2), (2009) 161-171.
[9] Kim, N. Il, & Lee, J., 'Geometrically nonlinear isogeometric analysis of functionally graded plates based on first-order shear deformation theory considering physical neutral surface', *Composite Structures*, **153**, (2016) 804-814.
[10] Nguyen-Xuan, H., Tran, L. V., Thai, C. H., Kulasegaram, S., & Bordas, S. P. A., 'Isogeometric analysis of functionally graded plates using a refined plate theory', *Composites Part B: Engineering*, **64**, (2014) 222-234.
[11] Yin, S., Hale, J. S., Yu, T., Bui, T. Q., & Bordas, S. P. A., 'Isogeometric locking-free plate element: A simple first order shear deformation theory for functionally graded plates', *Composite Structures*, **118** (1), (2014) 121-138.
[12] Yu, T. T., Yin, S., Bui, T. Q., & Hirose, S., 'A simple FSDT-based isogeometric analysis for geometrically nonlinear analysis of functionally graded plates', *Finite Elements in Analysis and Design*, **96** (C), (2015) 1-10.
[13] Hughes, T.; Cottrell, J.; Bazilevs, Y., 'Isogeometric analysis: CAD, finite elements, NURBS, exact geometry and mesh refinement', *Computer Methods Applied Mechanics and Engineering*, v. **194**, (2005) p. 4135−4195.
[14] Piegl, L.; Tiller, W., 'The NURBS Book'**,** 2nd ed (Germany: Springer, 1997).
[15] Shen, H.S., 'Functionally graded materials: nonlinear analysis of plates and shells' (Boca Raton: CRC Press, 2009).
[16] Parente, E.; Holanda, A. S.; Silva, S. M. B. A., 'Tracing nonlinear equilibrium paths of structures subjected to thermal loading', *Computational Mechanics*, vol. **38**, pp. (2006) 505-520.
[17] SIMULIA. 'ABAQUS/Standard user's manual', Version 6.12 (Providence, RI, USA, 2012).
[18] Shen, H.S., 'Postbuckling Behavior of Plates and Shells', 1st ed (Singapore: World Scientific, 2017)
[19] Bateni, M., Kiani, Y. & Eslami, M. R., 'A comprehensive study on stability of FGM plates', *International Journal of Mechanical Sciences*, **75**, (2013) 134-144.